PROTEINS
STRUCTURE ■ FUNCTION ■ BIOINFORMATICS

STRUCTURE NOTE

Crystal structure of the *Mycobacterium tuberculosis* phosphate binding protein PstS3

Davide M. Ferraris,[1]* Ralf Spallek,[2] Wulf Oehlmann,[2] Mahavir Singh,[2] and Menico Rizzi[1]

[1] Department of Pharmaceutical Sciences, Università del Piemonte Orientale "A. Avogadro,", Largo Donegani 2, 28100 Novara, Italy

[2] LIONEX Diagnostics and Therapeutics GmbH, D-38126 Braunschweig, Germany

ABSTRACT

***Mycobacterium tuberculosis* evades host immune responses by colonizing macrophages. Intraphagosomal *M. tuberculosis* is exposed to environmental stresses such as reactive oxygen and nitrogen intermediates as well as acid shock and inorganic phosphate (Pi) depletion. Experimental evidence suggests that expression levels of mycobacterial protein PstS3 (Rv0928) are significantly increased when *M. tuberculosis* bacilli are exposed to Pi starvation. Hence, PstS3 may be important for survival of Mtb in conditions where there is limited supply of Pi. We report here the structure of PstS3 from *M. tuberculosis* at 2.3-Å resolution. The protein presents a structure typical for ABC phosphate transfer receptors. Comparison with its cognate receptor PstS1 showed a different pattern distribution of surface charges in proximity to the Pi recognition site, suggesting complementary roles of the two proteins in Pi uptake.**

Proteins 2014; 82:2268–2274.

Key words: tuberculosis; phosphate depletion; bacterial survival; two-component system; Pst system; protein refolding and crystallization; thermal shift assay; binding affinity.

INTRODUCTION

Tuberculosis (TB) is a widespread, severe human infectious disease caused by the bacterium *Mycobacterium tuberculosis* (Mtb) and is a leading cause of death and a major sanitary concern in developing countries. Mtb is able to prevent phagocytosis by alveolar macrophages and to survive in the host organism even for decades through the formation of a peculiar pulmonary structure (called granuloma) that engulf and preserve the bacteria in a dormant, nonvirulent state.[1] Under this condition Mtb is exposed to severe stresses such as hypoxia, reactive oxygen and nitrogen species, acidic stress and Pi depletion. The survival of Mtb under Pi depletion/starvation relies on the presence of phosphate-specific transport (Pst) system responsible for Pi sensing and import and ultimately for bacterial survival.[2] The Pst system is constituted by three periplasmic PstS proteins (PstS1, PstS2 and PstS3) responsible for binding and scavenging extracellular Pi, by the trasmembrane proteins PstA and PstC that form the channel for Pi entry, and by PstB that provides energy for transport via ATP hydrolysis. All the components of the Pst system form an adenosine-5′-triphosphate (ATP) binding cassette (ABC) transporter important for sequestration and import of extracellular Pi.[3]

Grant sponsor: European Union FP7 Program; Grant number: SysteMTb HEALTH-F4-2010-241587.
*Correspondence to: Davide M. Ferraris, Department of Pharmaceutical Sciences, Università del Piemonte Orientale "A. Avogadro," Largo Donegani 2, 28100 Novara, Italy. E-mail: davide.ferraris@pharm.unipmn.it
Received 4 October 2013; Revised 20 February 2014; Accepted 4 March 2014
Published online 11 March 2014 in Wiley Online Library (wileyonlinelibrary.com). DOI: 10.1002/prot.24548

In Mtb all the genes coding for the Pst complex are coded by the Pho regulon, a global regulatory network involved in bacterial Pi management and survival under Pi-limited conditions. The Pho regulon is subdivided in four clusters: the *phoT* cluster, the *pstB-pstS1-pstC1-pstA2* cluster, the *pstS2-pknD* cluster and the *pstS3-pstC2-pstA1* cluster.[3] Variation of Pi concentrations influence the regulation of the transcription of all the above gene clusters and determine the robust upregulation of *pstS3-pstC2-pstA1* cluster following Pi starvation, being the *pstS3* gene the most upregulated. Moreover, Mtb *psts3* knockout mutant showed more susceptibility to Pi starvation in terms of bacterial growth and metabolic activity compared to wild-type Mtb.[3] Together, these results underline the critical role of PstS3 for Mtb survival in Pi-limited environment and possibly the important role of PstS3 in Mtb pathogenicity.

In this study we present the crystal structure of Mtb PstS3 at 2.3-Å resolution. The structure is similar to other homologous ABC phosphate transfer receptors. However, peculiar surface charge distribution in proximity of the ligand-binding site, different from the already characterized *M. tuberculosis* PstS1, lead to speculation about the role of the two cognate proteins in Pi uptake. In addition, we report the affinity constant of PstS3 for the phosphate ion calculated using the thermal shift assay method.

MATERIALS AND METHODS

Protein Expression and Purification

The PstS3-encoding gene was cloned in the pET22 vector using the *Nde*I and *Bam*HI restriction sites upstream to a 6xHis-tag coding region. The expression vector was transformed in *E. coli* Rosetta (DE3) cells (Novagen). For PstS3 expression, the cells were grown in LB medium at 37°C, induced with a final concentration of 1 mM IPTG at an OD_{600} of 1 and incubated at 37°C for 4 h. After centrifugation at 6000*g* for 15 min at 4°C the cells were suspended in 50 m*M* potassium phosphate buffer, pH 7.3 (Buffer A). The cells were disrupted using a Miccra D-8 homogenizer with a PF/MIR disperging tool (ART Prozess- & Labortechnik GmbH) at 23,500 min^{-1} for 30 s followed by sonication for 3 × 1 min using a Bandelin GM70 sonifier with SH70G/TT13 tip at output level 80%. After another centrifugation the pellet was resuspended in Buffer A followed by homogenization and centrifugation as described above. Pelleted inclusion bodies were washed with Buffer B (50 m*M* potassium phosphate buffer, 100 m*M* NaCl, pH 7.3) supplemented with 3*M* urea. After centrifugation the pellet was solubilized in Buffer B in which 8*M* urea and 5 m*M* imidazole were added. After another centrifugation at 27,500*g* for 30 min at 4°C the supernatant obtained was subjected to an affinity chromatography on Ni-NTA Superflow resin (Qiagen). Denatured PstS3 was eluted in a linear imidazole gradient from 5 to 300 m*M* imidazole. PstS3-containing fractions were pooled and diluted to a concentration of 100 μg mL^{-1} with Buffer B supplemented with 8*M* urea, 5 m*M* imidazole, and 20 m*M* DTT. The protein solution was refolded by buffer exchange on a Sephadex G25 column (GE Healthcare) into Buffer C (25 m*M* potassium phosphate buffer, pH = 7.3). The protein containing high molecular weight fraction of this gel filtration step was collected and subjected to another affinity purification step on Ni-NTA Superflow resin (Qiagen). After loading the protein the column was washed with Buffer C supplemented with 100 m*M* imidazole followed by an elution step using Buffer C and 500 m*M* imidazole. The fractions containing pure PstS3 protein were pooled. The protein solution underwent another buffer exchange step on a Sephadex G25 column (GE Healthcare) into 10 m*M* NH_4HCO_3, pH = 8.0. The protein containing high molecular weight fraction of this gel filtration step was collected and applied on a preparative Superdex^{TM} 200 column (GE Healthcare) using 20 m*M* tris, pH = 8.0 as running buffer. The monomeric fraction of PstS3 deriving from this gel filtration was collected and concentrated using polyethersulfone membranes with 10 kDa cut-off (Vivaspin 20, Sartorius stedim biotech).

Crystallization

Purified PstS3 was concentrated to 1.8 mg mL^{-1} and first crystallization trials were carried out using Crystal Screen I and Crystal Screen II (Hampton), Classics Suite I and Classsics Suite II and MBClass (Qiagen) screens. An automated dispensing robot (Douglas Instruments) and 96-well MRC 2 Well Crystallization Plate (Swissci) were employed for crystallization experiments. Protein/reservoir solutions were mixed in 50/50 and 75/25 ratios with a final drop volume of 800 nL and incubated at 20°C against a reservoir volume of 40 μL. Crystals grew in several conditions after few days. Small, aggregated needles and wisps were the dominant crystal morphologies and growth patterns. Single, intergrown crystals were obtained in condition 22 of Hampton Crystal Screen II (0.1 *M* MES monohydrate pH = 6.5, 12% w/v PEG 20000) in 50:50 protein/reservoir ratio drops. Single, brick-shaped, diffraction quality crystals were obtained in this conditions by adding NaH_2PO_4 at a final concentration of 0.5 m*M* to the protein solution prior to protein crystallization. Crystals grew to full size after 1-month incubation at 20°C. For diffraction analysis, crystals were fished, cryoprotected with 15%(w/v) glycerol and flash-frozen in liquid nitrogen for later crystallographic analysis.

X-Ray Data Collection, Structure Determination, and Refinement

Diffraction datasets were collected on the ID29 beamline at the Electron Synchrotron Research Facility (ESRF)

Table I
Data Collection and Refinement Statistics

Beamline	ESRF ID29
Space group	$P2_1$
Unit cell dimensions (Å), (°)	$a = 36.21$, $b = 229.25$, $c = 39.10$; $\alpha = 90.00$, $\beta = 100.03$, $\gamma = 90.00$
Resolution (Å)	38.51–2.30 (2.39–2.30)
Completeness (%)	97.0 (92.8)
Multiplicity	3.0 (3.1)
Total reflections	81,631 (8227)
Unique reflections	26.706 (2635)
Mean $I/\sigma(I)$	5.5 (3.4)
R_{merge}	0.174 (0.336)
Molecules per asymm. unit	2
Solvent content (%)	51.0
Wilson B factor (A^2)	21.8
Refinement statistics	
R/R_{free}	0.238/0.278 (0.299/0.342)
R.m.s. deviation	
Bonds (Å)/Angles (°)	0.010/1.56
Ramachandran plot	
Residues in favoured regions (%) (number of residues)	96.1 (609/634)
Residues in allowed regions (%) (n. residues/total)	99.8 (633/634)
Residues in outlier regions (%) (n. residues/total)	0.16 (1/634)

Statistics for the highest-resolution shell are shown in parentheses.

in Grenoble, France. Best-diffracting data collection wedges of two isomorphous crystals grown in the same drop were used for collection of a complete dataset. Diffraction images were processed using the *CCP4* software suite.[4] PstS3 crystals belonged to space-group $P2_1$ with unit-cell parameters $a = 36.21$ Å, $b = 229.25$ Å, $c = 39.10$ Å; $\alpha = 90.00°$, $\beta = 100.03°$, $\gamma = 90.00°$. Two monomers are present in the asymmetric unit, giving a Matthews parameter and solvent fraction of 2.53 $Å^3$ Da^{-1} and 51.0%, respectively. Space group $P2_1$ was selected based on the indexing scores given by the automatic indexing processes of *MOSFLM* and *XDS*, the observed systematic absences and the favorable R_{meas} values obtained for the selected space group. Molecular replacement was performed using *PHASER*[5] included in the *PHENIX* software suite[6] and using the structure of phosphate binding protein (PBP) from *Escherichia coli* as the search model (Protein Data Bank ID code 2ABH). Initial crystallographic refinement carried out with *REFMAC*[7] and *PHENIX*[6] gave relatively high R factor values (0.230/0.302 for R/R_{free}, respectively), suggesting a possible data problem. Analysis of crystal twinning conducted using the L-test twinning analysis of the program *TRUNCATE* of the CCP4 suite[4] indicated the presence of partial twinning with a twin fraction of 0.18. Structure refinement was then performed using amplitude-based twin refinement of the program *REFMAC* of the *CCP4* suite.[4] The program identified the twin operator L, -K, H and a twin fraction of 0.12. The twin operator indicates a rare type of pseudo-merohedral twinning occurring in monoclinic systems where a and c axis are equal or, as in the case of PstS3 crystals, close enough in length to mimic a C-centered orthorhombic cell. However, data processing in $C222_1$ failed due to unacceptable high R_{meas} values, probably because of the insufficient length similarities of the a and c axes. Final refinement was performed with *phenix.refine* of the *PHENIX* suite[6] using L, -K, H as the twin law. The program calculated a twin fraction of 0.16, and the structure was refined to final R/R_{free} values of 0.238/0.278, respectively, with good geometry (Table I). The final model consists of 638 protein residues, 179 solvent molecules and two Pi groups (one per PstS3 molecule).

Thermal Shift Assay

The reaction mix used in the thermal-shift assay consisted of the PstS3 protein diluted to a final concentration of 0.2 mg mL^{-1} in a buffer containing 20 m*M* Tris pH = 8 and mixed with an appropriate amount of a stock solution of 100 m*M* Na_2HPO_4 pH = 8 and with the fluorescence probe SYPRO® Orange (Sigma–Aldrich) used at 1/4000 dilution. The final reaction volume was 20 µL. Fluorescence was recorded in a 48-well plate using the FAM channel of a MiniOpticon™ Real-Time PCR Detection System (Bio-Rad). The protein–ligand affinity constant (K_d) was calculated by measuring the concentration-dependent effects of Pi on the protein melting temperature (T_m), as described by Matulis *et al.*[8] Data were harvested and analyzed using CFX Manager™ Software (Bio-Rad) and SigmaPlot (Systat Software, San Jose, CA, www.sigmaplot.com).

RESULTS

Overall PstS3 Structure

Mtb PstS3 folds into an elongated curved structure composed of two globular α/β lobes. At the interface of the two lobes is located the surface-exposed cleft hosting the Pi recognition site [Fig. 1(A)]. Overall, the structure is bent toward the ligand binding site giving to PstS3 the typical "Venus flytrap" fold previously observed in other phosphate ABC transporters and DING proteins.[9–11] This curved fold is typical of this protein class and is the result of the movements of the two lobes towards the Pi binding site upon ligand binding.

Structure and sequence alignment analysis [Fig. 1(B)] reveals that Mtb PstS3 shares high structure similarity with Mtb PstS1 (rmsd = 1.85 Å, 30% sequence identity),[10] with PBP from *E. coli* (rmsd = 1.84 Å, 31% sequence identity)[9] and with the DING protein PfluDING from *P. fluorescens* (rmsd = 1.84 Å, 28% sequence identity).[11]

A major disorder features the N-terminal region of the protein, where electron density corresponding to the first

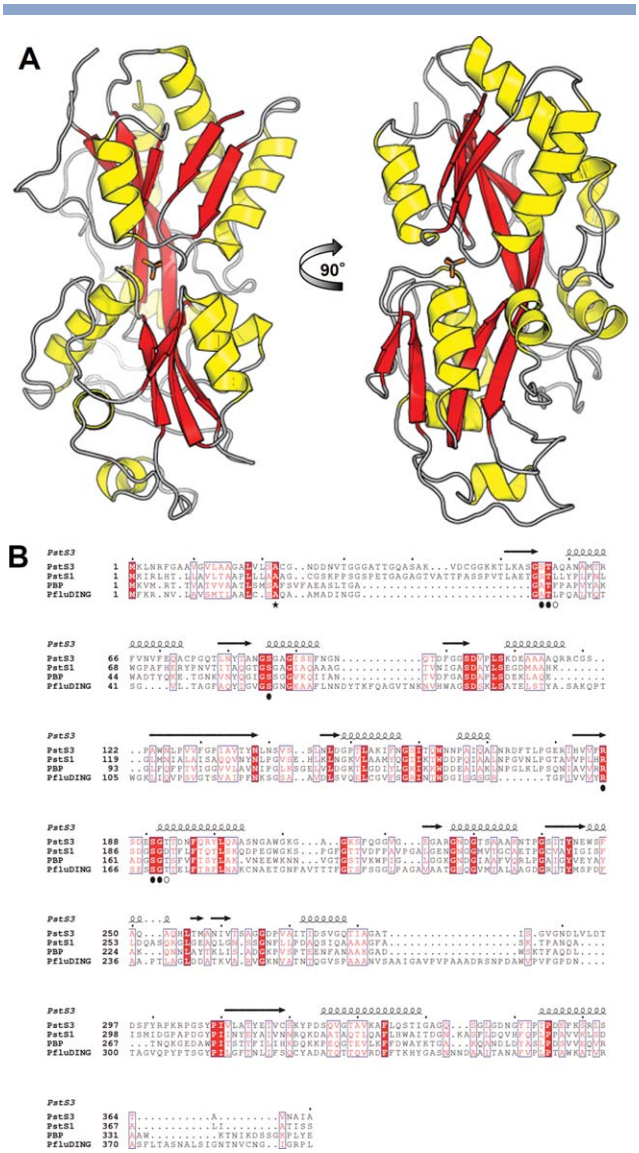

Figure 1

(**A**) Left: structure of PstS3 from *M. tuberculosis*. α-helices are represented with yellow ribbons; β-sheets are represented with red ribbons. Phosphate ion is shown in sticks. Right: clockwise rotation of PstS3 structure by 90° along its major axis. (**B**) Sequence alignments of PstS3 with PstS1 from *M. tuberculosis*, PBP from *E. coli*, and PfluDING from *P. fluorescence*. Red boxes with white characters indicate residue identity; red characters indicate residue similarity; blue-framed characters indicate similarities between groups of residues. Conserved residues that bind phosphate ion are indicated with black circles; nonconserved residues that bind phosphate are indicated with white circles. Predicted position of signal sequence cleavage is indicated with a black star. PstS3 secondary structure is shown on top of the sequence alignment.

50 amino acids is missing. PstS3 is an extracellular-targeted protein bearing at the N-terminus an export sequence and a signal sequence cleavage site between positions 22 and 23. The PstS3 signal sequence is necessary for extracellular localization of the protein and it is cleaved upon export. N-terminal sequencing and MALDI-TOF analysis of the purified protein showed a major amino acid sequence beginning at position 21 (data not shown).

Interactions of PstS3 with Phosphate

The phosphate ion is held in place by a network of 12 hydrogen bonds [Fig. 2(A,B)]. Oxydryl groups of residues Ser56 and Thr57 act as proton donor to phosphate O4 (2.95 Å) and O1 (3.22 Å), respectively. The main chain NH groups of Thr57 and Ala58 form hydrogen bonds with respectively the Pi atoms O1 (2.67 Å) and O4 (2.63 Å). The Arg187 guanidinium group is engaged in hydrogen bonds with O1 (2.86 Å) and O2 (2.66 Å). Furthermore, the Pi O2 atom is hydrogen bonded to the Thr193 main chain NH and Oγ atoms (3.08 Å and 2.71 Å, respectively) and to the Oγ of Ser191 (2.76 Å). In total, O2 of the complexed phosphate engages in four hydrogen bonds occurring in the rare pyramidal geometry already observe in PBP.[9] Finally, O3 receives protons from the main chain NH of Gly192 (2.56 Å) and of Ser86 (3.09 Å). Analogously to Ser56, Ser86 donates a proton to O3 through its oxydryl Oγ (2.77 Å).

PstS3 Surface Charge Distribution

PstS3 presents a predominantly negatively charged surface along with scattered patches of positively charged residues [Fig. 2(C)]. This differs from what observed in the Mtb homologous protein PstS1, where an entirely negatively charged surface in proximity of the ligand-binding site is observed. The difference in charge distribution surrounding the Pi recognition site could influence the ligand binding kinetics of the two proteins, leading to speculations over the role of the two proteins in Pi uptake, as discussed later.

Determination of PstS3 Pi Affinity

We determined the affinity constant of PstS3 for its natural ligand Pi. For this purpose we used the thermal shift method as described by Matulis *et al.*[8]

Figure 2(D) shows the change in T_m following addition of 1 m*M* Pi to PstS3. A significant variation of Tm shift is observed, changing from 66.2°C of the ligand-free protein to 78.0°C of the ligand-bound (ΔT_m = 11.8°C). Figure 2(E) shows the variation of PstS3 Tm caused by addition to the protein solution of Pi at increasing concentrations. The calculated K_d of PstS3 toward Pi was 64.8 μ*M*.

DISCUSSION

We report the crystal structure of the recombinant Mtb extracellular phosphate-binding protein PstS3 purified from inclusion bodies. The overall structure and the specific interactions of PstS3 with the phosphate ion are very similar to that observed in other ABC transporter

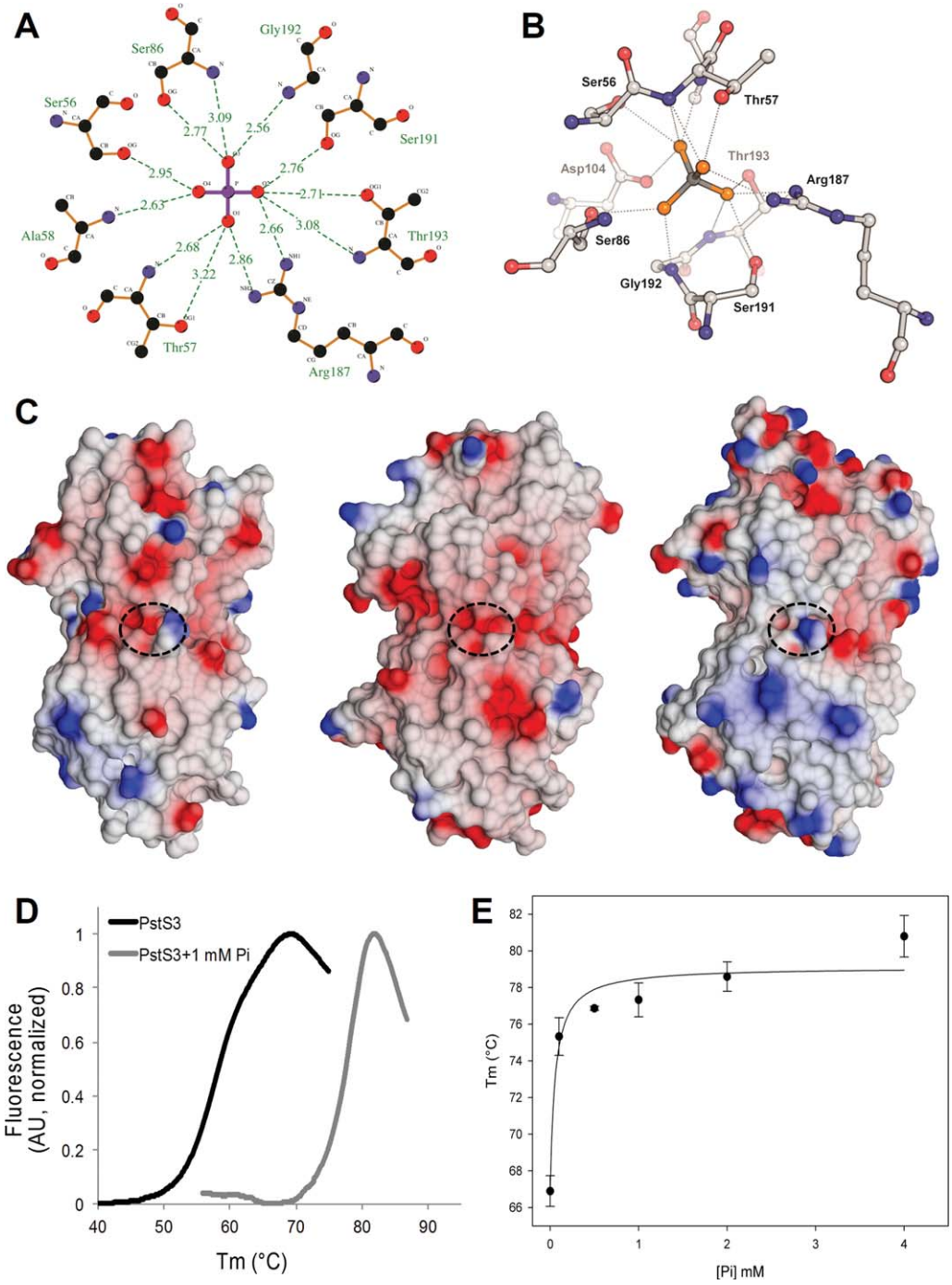

Figure 2

(**A**) Schematic representation of phosphate ion interactions with PstS3. (**B**) Balls and sticks representation of PstS3 residues interacting with phosphate. (**C**) Electrostatic surface of PstS3 (left), PstS1 (center) and PBP (right) calculated and displayed using CCP4mg. The surface potentials displayed scale from −0.5 V (red, negatively charged) to +0.5 V (blue, positively charged). (**D**) Normalized melting curves of PstS3 with and without addition of Pi (light grey curve and black curve, respectively). (**E**) Variation of PstS3 Tm at increasing Pi concentration.

phosphate receptors of the same and other organisms, thus allowing to draw analogies over the role of key residues of the PstS3 recognition site in Pi specificity and selectivity.

PstS3 Phosphate Specificity and Selectivity

In the first reported crystal structure of the phosphate-transport protein PBP[9] the authors suggested the ability of PBP to bind monobasic ($H_2PO_4^-$) and dibasic

(HPO_4^{2-}) phosphate species. It has been later proved that the ability of phosphate binding for PtsS3 homologous proteins PstS1 and PBP is not greatly altered in pH intervals ranging from 4.3 to 8.5, suggesting their ability to bind monobasic and dibasic phosphate species.[12] As for other phosphate-binding proteins of the same family, a key role for binding monobasic and dibasic phosphate species relies on the presence, in PstS3, of residue Asp104. Under acidic conditions, Asp104 is able to accept a proton from neighbor Ser86 Oγ (3.22 Å), thus allowing the second proton to be shared between the O4 of the phosphate ion and the Oγ of Ser86. The resulting negative charge present on the two oxygen molecules O1 and O2 is complemented by the positive charge of Arg187.

Binding of dibasic phosphate species is slightly favoured under basic conditions.[9] In this environment, the proton of Ser86 Oγ is shared between the nonprotonated phosphate O3 and Asp104 Oδ. Thus, Asp104 plays a major role in PstS3 mono- and di-basic phosphate binding by accepting and/or sharing protons according to the phosphate ions involved. The ability of PstS3 to bind monobasic and dibasic phosphate constitutes a great advantage for bacterial survival especially in environments where phosphate supply is limited. Moreover, Asp104 has a key role in discriminating closely related species such as phosphate and sulfate: both ions have a tetrahedral geometry; however, the sulfate ion, differently from phosphate, is not protonated and bears negative charges, and would be repelled by the presence of the partial negative charge of Asp104 carboxylic group. In PBP this conserved Asp residue has been shown to be responsible for the discrimination of phosphate from sulfate by five orders of magnitude.[9]

PstS3 Surface Charge Distribution and Ligand Selectivity

PstS3 structure analysis reveals a concentration of negatively charged residues in proximity of the ligand-binding site surrounded by scattered patches of positively charged residues. This differs from what observed in PstS1, where an entirely negatively charged surface is observed [Fig. 2(C)]. Intuitively, the presence of negative surface charges would discourage the approach of negative species to the phosphate recognition site, thus hampering phosphate binding. However, Ledvina *et al.* demonstrated that local short-distant charges complementarity are more important for ligand binding than long distance charge repulsions.[13] In support to this theory, computational simulations conducted by Huang and Briggs demonstrated that the scattered, positively charges patches above and below the ligand binding entrance site are the major contributors to ligand attraction toward the Pi recognition site.[14] On the same line, Held *et al.*[15] used computational dynamics and modelling to demonstrate that the binding of the phosphate species occur through a two-step "catch-and-select" mechanism, where the anionic ligand species are: (1) nonspecifically selected on the protein surface and directed toward the ligand binding site through the presence of scattered anion attractors sparsely located on the protein surface, and (2) specifically selected in the ligand binding site among the various ionic species due to a series of precise interactions. Therefore, the presence of a negatively charged surface in combination with scattered patterns of charged residues constitutes an advantage in terms of substrate selectivity.

Hence, the observed differences in PstS1 and PtS3 in the type and distribution of surface charges in proximity to the ligand binding site suggest the complementary role of the two proteins in binding phosphate ions following a mechanism determined mainly by different ligand binding kinetics rather than by mere specificity. This could constitute an advantage when Mtb bacteria need to scavenge extracellular phosphate in environments where different pH values, ionic forces and competitive anions are present. In addition, the suggested complementary role of PstS1 and PstS3 in phosphate binding could constitute an ever-functioning scavenging system that may be vital for assuring a continuous supply of phosphate and the bacterial survival in the particular severe conditions faced by Mtb in the early stages of the infection.

REFERENCES

1. Chan J, Flynn J. The immunological aspects of latency in tuberculosis. Clin Immunol 2004;110:2–12.
2. Peirs P, Lefevre P, Boarbi S, Wang XM, Denis O, Braibant M, Pethe K, Locht C, Huygen K, Content J. *Mycobacterium tuberculosis* with disruption in genes encoding the phosphate binding proteins PstS1 and PstS2 is deficient in phosphate uptake and demonstrates reduced in vivo virulence. Infect Immunol 2005;73:1898–1902.
3. Vanzembergh F, Peirs P, Lefevre P, Celio N, Mathys V, Content J, Kalai M. Effect of PstS sub-units or PknD deficiency on the survival of *Mycobacterium tuberculosis*. Tuberculosis (Edinb) 2010;90:338–345.
4. Winn MD, Ballard CC, Cowtan KD, Dodson EJ, Emsley P, Evans PR, Keegan RM, Krissinel EB, Leslie AG, McCoy A, McNicholas SJ, Murshudov GN, Pannu NS, Potterton EA, Powell HR, Read RJ, Vagin A, Wilson KS. Overview of the CCP4 suite and current developments. Acta Crystallogr D Biol Crystallogr 2011;67 (Part 4):235–242.
5. McCoy AJ, Grosse-Kunstleve RW, Adams PD, Winn MD, Storoni LC, Read RJ. Phaser crystallographic software. J Appl Crystallogr 2007;40 (Part 4):658–674.
6. Adams PD, Afonine PV, Bunkoczi G, Chen VB, Davis IW, Echols N, Headd JJ, Hung LW, Kapral GJ, Grosse-Kunstleve RW, McCoy AJ, Moriarty NW, Oeffner R, Read RJ, Richardson DC, Richardson JS, Terwilliger TC, Zwart PH. PHENIX: a comprehensive Python-based system for macromolecular structure solution. Acta Crystallogr D Biol Crystallogr 2010;66 (Part 2):213–221.
7. Murshudov GN, Vagin AA, Dodson EJ. Refinement of macromolecular structures by the maximum-likelihood method. Acta Crystallogr D Biol Crystallogr 1997;53 (Part 3):240–255.

8. Matulis D, Kranz JK, Salemme FR, Todd MJ. Thermodynamic stability of carbonic anhydrase: measurements of binding affinity and stoichiometry using ThermoFluor. Biochemistry 2005;44:5258–5266.
9. Luecke H, Quiocho FA. High specificity of a phosphate transport protein determined by hydrogen bonds. Nature 1990;347:402–406.
10. Vyas NK, Vyas MN, Quiocho FA. Crystal structure of *M. tuberculosis* ABC phosphate transport receptor: specificity and charge compensation dominated by ion-dipole interactions. Structure 2003;11: 765–774.
11. Liebschner D, Elias M, Moniot S, Fournier B, Scott K, Jelsch C, Guillot B, Lecomte C, Chabriere E. Elucidation of the phosphate binding mode of DING proteins revealed by subangstrom X-ray crystallography. J Am Chem Soc 2009;131:7879–7886.
12. Wang ZM, Luecke H, Yao NH, Quiocho FA. A low energy short hydrogen bond in very high resolution structures of protein receptor phosphate complexes. Nat Struct Biol 1997;4:519–522.
13. Ledvina PS, Tsai AL, Wang Z, Koehl E, Quiocho FA. Dominant role of local dipolar interactions in phosphate binding to a receptor cleft with an electronegative charge surface: equilibrium, kinetic, and crystallographic studies. Protein Sci 1998;7:2550–2559.
14. Huang HC, Briggs JM. The association between a negatively charged ligand and the electronegative binding pocket of its receptor. Biopolymers 2002;63:247–260.
15. Held M, Metzner P, Prinz JH, Noe F. Mechanisms of protein-ligand association and its modulation by protein mutations. Biophys J 2011;100:701–710.